photonics

MDPI

Article

Observation of Giant Angular Goos-Hanchen Shifts Enhanced by Surface Plasmon Resonance in Subwavelength Grating

Nikolai I. Petrov [1,*], Yuri M. Sokolov [1], Vladimir V. Stoiakin [1], Viktor A. Danilov [1], Vladimir V. Popov [2] and Boris A. Usievich [3]

[1] Scientific and Technological Centre of Unique Instrumentation, Russian Academy of Sciences, 117342 Moscow, Russia
[2] Faculty of Physics, Lomonosov Moscow State University, 119991 Moscow, Russia
[3] Prokhorov General Physics Institute, Russian Academy of Sciences, 119991 Moscow, Russia
* Correspondence: petrovni@mail.ru

Abstract: The effect of the Goos-Hanchen (GH) angular shift for a visible light beam under the excitation of surface plasmon resonance (SPR) in a metal subwavelength grating has been investigated. Extremely large angular GH shifts have been demonstrated for a subwavelength grating with an optimal depth. The high sensitivity of the beam shape transformation and the GH shift to a change in the angle of incidence near the SPR has been shown by rigorous electromagnetic simulation and demonstrated experimentally. The focusing of the reflected beam near the subwavelength grating surface has been demonstrated.

Keywords: subwavelength grating; surface plasmon resonance; angular Goos-Hanchen shift

check for updates

Citation: Petrov, N.I.; Sokolov, Y.M.; Stoiakin, V.V.; Danilov, V.A.; Popov, V.V.; Usievich, B.A. Observation of Giant Angular Goos-Hanchen Shifts Enhanced by Surface Plasmon Resonance in Subwavelength Grating. *Photonics* **2023**, *10*, 180. https://doi.org/10.3390/photonics10020180

Received: 9 January 2023
Revised: 26 January 2023
Accepted: 3 February 2023
Published: 8 February 2023

1. Introduction

The beam reflected off an interface experiences spatial and angular shifts depending on its polarization and profile. The spatial displacements constitute the well-known Goos-Hänchen (GH) shift in the plane of incidence [1,2]. In [3], the first observation of the GH shift of a light beam incident on a bare metal surface was reported. The physical origin of the lateral GH shift lies in the angular dispersion of the Fresnel reflection coefficients. The phase changes of plane waves with different wavenumbers combine together to generate the GH shift. Usually, the GH shift is of the order of the wavelength. Detecting such a small GH shift is not an easy task, so significant increase is necessary for practical applications. Various methods to enhance the shifts were considered. The displacement of the order of the beam width was shown for multilayered structures in [2]. Significant enhancement of the GH shift is obtained by the excitation of surface plasmon waves on metal surfaces [4–6] and Bloch surface electromagnetic waves in photonic crystals [7]. Different materials and structures were considered to enhance the GH effect. The enhancement has been shown using weakly absorbing slabs [8], gradient meta-surfaces [9], subwavelength gratings [10], graphene [11] and a coherent medium [12]. In [13], beam shifts or corrections with respect to geometrical optics caused by the wave effects in a graded-index optical fiber were investigated. An angular shift of a beam at an air–glass interface was experimentally demonstrated in [14]. A noticeable increase in angular displacement can be observed for a tightly focused beam reflected by a dielectric interface near the Brewster angle [15]. The existence of large positive and negative GH shifts in photonic crystal mirrors was demonstrated in [16]. In [17], the negative GH shift on a two-dimensional photonic crystal with an effective negative refractive index was investigated by simulation and experiment.

Recently, the composite GH shifts have been investigated and experimentally observed at the air–Au interface [18]. The composite GH shift of a Gaussian optical beam reflected at a glass–air interface in the visible and near-infrared regimes was experimentally investigated [19]. The combined effect of the GH shift and the angular deviations

generated by the transmission through the incoming and outgoing interfaces of the triangular prism was also analyzed [20]. The spatial and angular GH and Imbert-Fedorov (IF) shifts of *p*-polarized light are significantly enhanced around the resonant angle of SPR. The enhanced temperature-dependent composite GH and IF shifts were employed for temperature sensing [21].

Large lateral displacements of beams incident upon a diffractive structure under resonance conditions can also be observed [5]. Large GH effects are also expected for dielectric gratings [4]. The GH angular shifts of several hundred microradians reinforced by the excitation of the SPR in a dielectric grating on a gold surface were demonstrated in [22]. However, the effects of the incident beam width and subwavelength grating height on the plasmon enhanced GH shifts have not yet been studied.

In this paper, we investigate the GH shift when the surface plasmon resonance is excited in a subwavelength nickel grating with a period Λ = 400 nm (Figure 1). The effects of angular shift and beam shape change on the reflected beam near the surface plasmon resonance condition are demonstrated experimentally and confirmed by rigorous electromagnetic simulations. A significant increase in the angular GH shift is achieved at an optimal grating depth h = 80 nm and a resonance angle of incidence $\theta_i = 33.53°$, corresponding to the optimal condition for the coupling of incident light with a surface plasmon. A significant increase in the angular shift with a decrease in the width of the incident beam is shown.

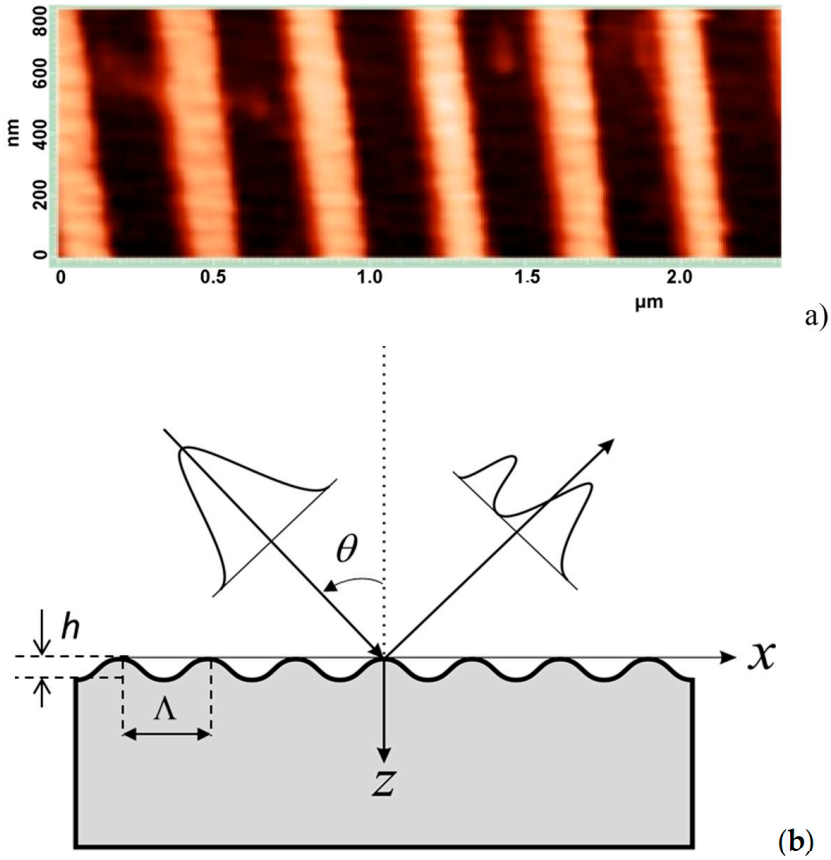

Figure 1. Image of grating (**a**) and reflection of a Gaussian beam by a metallic grating (**b**).

2. Surface Plasmon Resonance in Subwavelength Grating

A rigorous electromagnetic theory based on the *C*-method is used for the calculations [23]. Note that an *s*-wave does not excite surface plasmon waves, so we consider the GH shift only for a *p*-polarized incident wave.

The angle of incidence θ_i, corresponding to the plasmon resonance, is determined by [10,24,25]:

$$sin\theta_i + m\frac{\lambda}{\Lambda} = \pm\sqrt{\frac{\varepsilon_r}{\varepsilon_r + 1}}, \quad (1)$$

where θ_i is the angle of incidence, λ is the wavelength, m is an integer, Λ is the grating period and ε_r, is the real part of the dielectric constant of a grating.

Figure 2 presents the diffraction efficiencies of *Ni* gratings with a period Λ = 400 nm depending on the angle of incidence for different grating depths.

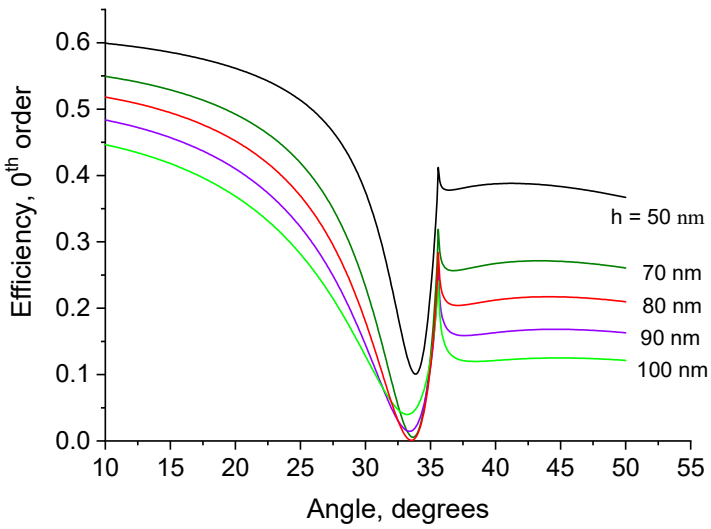

Figure 2. Calculated diffraction efficiencies of the zero-order depending on the angle of incidence for the nickel grating with a period Λ = 400 nm and different depths h = 50, 70, 80, 90, 100 nm at a wavelength of radiation λ = 632.8 nm with p-polarization.

It can be seen that the Wood and Rayleigh anomalies [26] occur at the corresponding incidence angles. The minimum zero reflection is achieved when the grating depth h becomes h_{opt} = 80 nm. This indicates that there is an effective coupling to the plasmon wave. As the grating depth decreases or increases relative to the optimal depth, the value of the minimum reflection coefficient increases. Note that the optimal depth depends on the grating material. It was shown in [10] that the optimal depth for the silver grating is h = 20 nm. The optimal grating depth, similar to the optimal thickness of the metal layer observed in [6], corresponds to the excitation of the surface plasmon where the resonant absorption is just balanced by radiation damping and internal damping. The minimum in the reflectance is due to destructive interference between the leakage radiation and the reflected part of the excitation beam. The absorption and radiative losses determine the width of the SPR: $\Gamma = \Gamma_{abs} + \Gamma_{rad}$. The absorption losses are defined by the material dispersion $\Gamma_{abs} = Im(k_{SP})$, while the radiative losses Γ_{rad} depend on the grating profile and increase with an increase in depth h [27]. It can be shown that the minimum reflection is achieved if the radiation loss is equal to the damping due to absorption [27]. This corresponds to the optimal coupling of the incident beam to the plasmon.

The absorption losses are defined by the imaginary part of the SP wave vector:

$$\Gamma_{abs} = Im(k_{SP}) = Im\left(k_0\sqrt{\frac{\varepsilon}{\varepsilon + 1}}\right) \approx 0.24\ \mu\text{m}^{-1},$$

where $\varepsilon = -10.1 + i14.731$ is the dielectric constant of nickel.

The radiation damping can be defined as $\Gamma_{rad} = 1/l_p \approx 0.3\ \mu\text{m}^{-1}$, where l_p is the plasmon path length. It follows from the calculations that the losses of the plasmons in a nickel grating with a period Λ = 400 nm and a depth h = 80 nm are equal to α = 3055 cm^{-1}. For a depth of h = 30 nm, plasmon losses are equal to 1500 cm^{-1} [10].

The minimum reflection is defined as $R_{min} = \left(\frac{\Gamma_{abs} - \Gamma_{rad}}{\Gamma_{abs} + \Gamma_{rad}}\right)^2 \approx 0.01$.

In Figure 3 the diffraction efficiencies of the *Ni* gratings depending on the angle of incidence for different radii w_0 of the incident beam are presented.

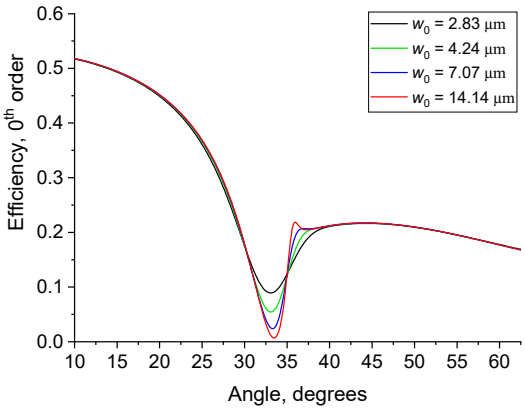

Figure 3. Calculated diffraction efficiencies of the zero-order depending on the angle of incidence for the nickel grating with a period Λ = 400 nm and depth h = 80 nm at a wavelength of radiation λ = 632.8 nm with p-polarization and different beam radii w_0 = 2.83 μm (black line), w_0 = 4.24 μm (green line), w_0 = 7.07 μm (blue line), w_0 = 14.14 μm (red line).

The influence of the incident beam width on the reflectivity is significant for the incidence angles at which plasmon resonance occurs. For highly focused beams, the effect of plasmon resonance is significantly reduced because of the fact that most of the angular components of the incident beam spectrum are not phase-matched with the surface plasmon modes. It was shown in [2] that the incident beam width should be greater than the propagation range of the surface plasmon mode in order to efficiently transfer energy to the plasmon field. The characteristic lengths l_p are determined by the losses of plasmons. In our case $l_p \approx 1/\alpha = 3.27$ μm. This indicates that the beam width w should be greater than 3.27 μm. Indeed, with a beam width of w_0 = 7 μm or more (Figure 3), almost all the incident power is absorbed by the grating, i.e., the incident energy is converted into surface plasmons.

In Figure 4a, the results of calculations and measurements of diffraction efficiency of the zero order of the nickel grating depending on the angle of incidence of the radiation with p-polarization are presented. It is seen that the effect of plasmon resonance occurs at the incidence angle of ~33° (Figure 4a). At a relief depth of h = 80 nm and incidence angle of $\theta_i = 33.53°$, almost all incident energy is absorbed by the grating (Figure 4a). Note that this depth corresponds to the plane wave minimum reflection at the resonance incidence angle.

It can be seen that zero reflection (Wood anomaly) is not achieved and the Rayleigh anomaly is less pronounced in measurements due to the finite angular convergence of the incident Gaussian beam.

In Figure 4b, the results of the calculation and measurements of diffraction efficiency of the zero order of the nickel grating with a period Λ = 400 nm and depth h = 40 nm depending on the angle of incidence of the radiation are presented. As can be seen, unlike a grating with a depth of h = 80 nm (Figure 4a), the reflectivity is significant even at a resonant incidence angle. This means that there is no effective transfer of incident energy to surface plasmons at a grating depth of h = 40 nm.

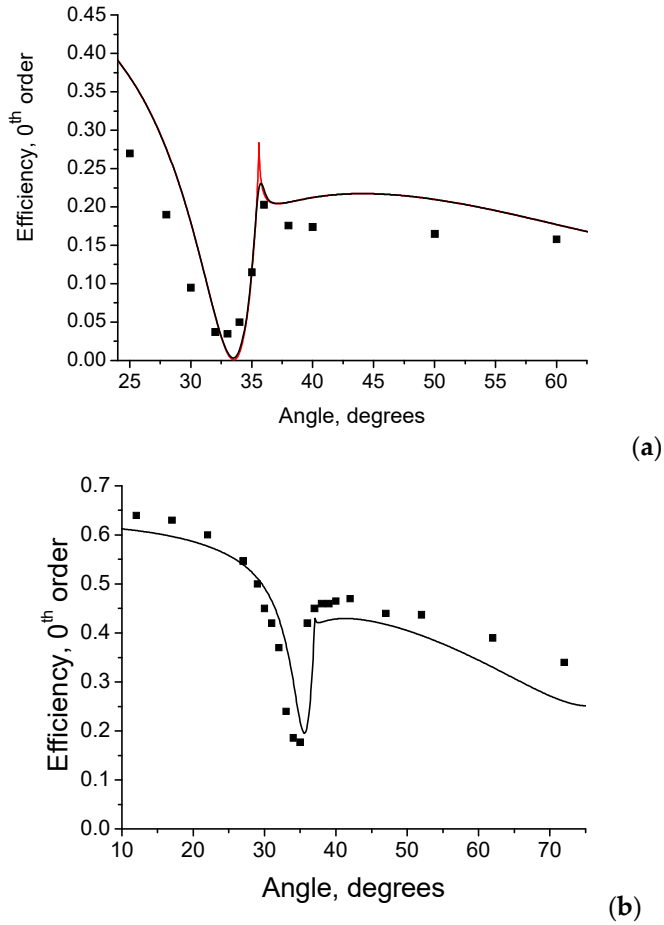

Figure 4. Calculated (solid lines: red—plane wave, black—Gauss beam with FWHM = 32 μm) and measured diffraction efficiencies of the zero-order depending on the incidence angle for the nickel grating with a period Λ = 400 nm and depths h = 80 nm (**a**) and h = 40 nm (**b**) at a wavelength of radiation λ = 632.8 nm with p-polarization.

Goos-Hanchen Shift

In Figure 5, the calculated intensity profiles of the reflected beam at a grating surface are presented under the surface resonance condition. While the negative lateral shift of the order of the beam radius occurs (Figure 5a), there is no angular shift (Figure 5b). Besides, the beam focusing in the reflection from the grating is also observed. It can be seen that the divergence angle of the reflected beam under the SPR condition almost two times larger than that of the incident beam $\Delta\theta_i \approx \lambda/\pi w_0 \approx 0.43^\circ$ (Figure 5b). Increase in the beam divergence angle is due to the beam reshaping at the grating surface.

Note that the effect of near-field beam focusing by a flat dielectric subwavelength grating was also demonstrated in [28].

In Figure 6 the angular intensity profiles of the reflected beam are presented for different values of the incident angle. It can be seen that the minimum intensity value in the dip corresponds to the incidence resonant angle because of the absorption of the field components with k_x corresponding to the SPR (Figure 6c). The transition between positive and negative angular shifts is observed when the angle of incidence deviates from the resonant one. When moving away from the resonant angle of incidence, only one reflected beam remains (Figure 6f). This indicates that, because of the existing shape of the reflection function (Figure 2), the components with higher spatial frequencies will mainly be reflected.

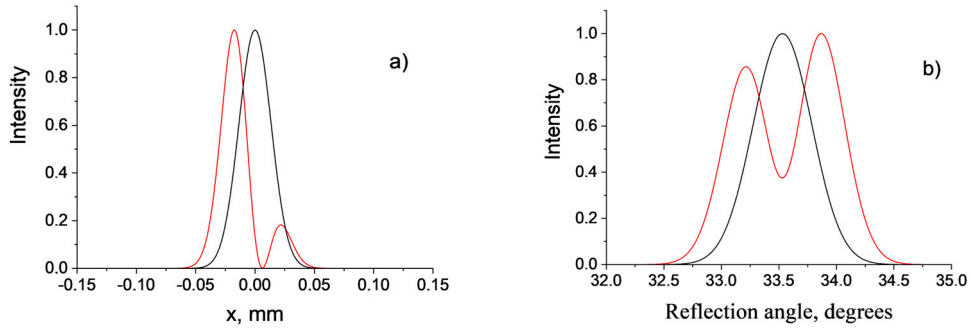

Figure 5. Normalized intensity profiles as function of the transverse coordinate (**a**) and reflection angle (**b**). Black lines—incident beam; red lines—reflected beams. Incident beam FWHM = 26.64 μm; $\theta_i = 33.53^\circ$; $z = 0$.

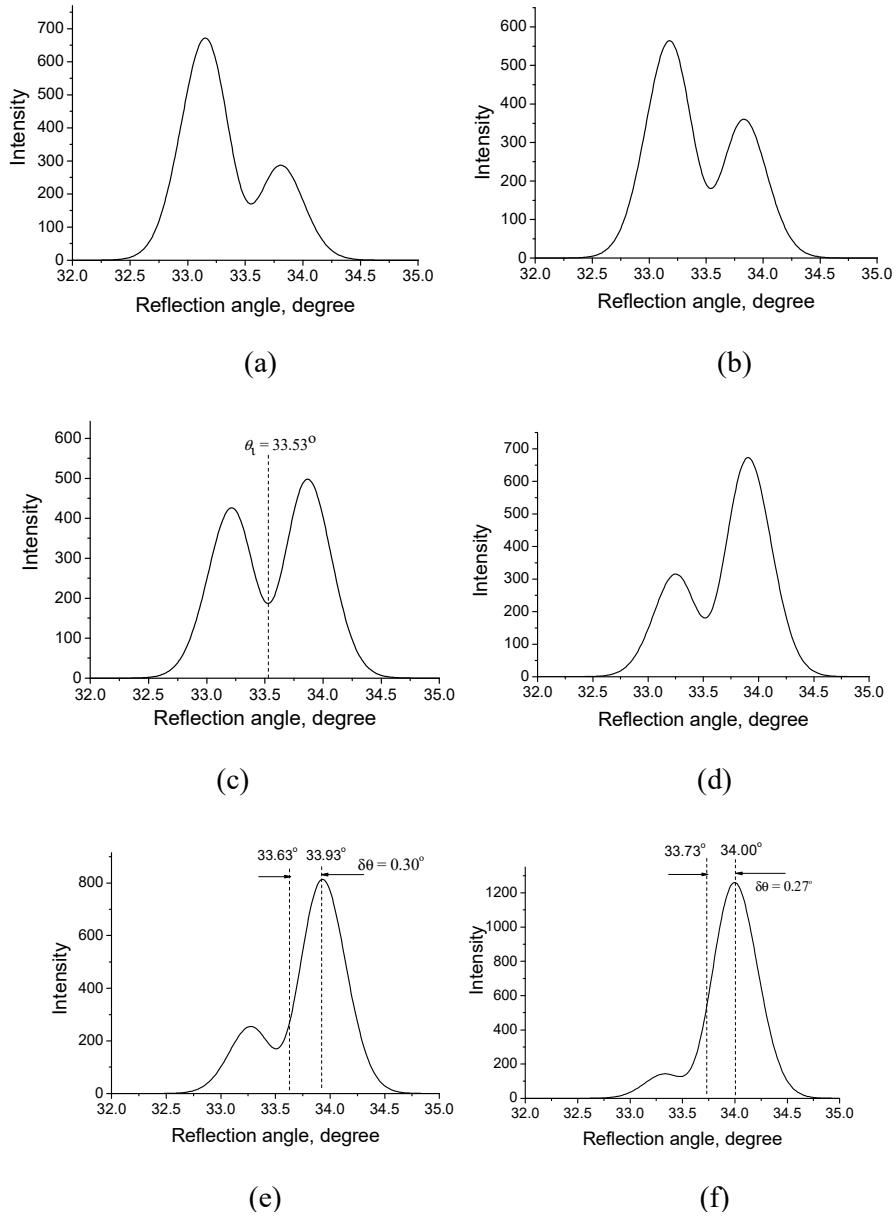

Figure 6. Calculated intensity profiles as function of the reflection angle. FWHM = 26.64 μm. (**a**) $\theta_i = 33.43^\circ$; (**b**) $\theta_i = 33.47^\circ$; (**c**) $\theta_i = 33.53^\circ$; (**d**) $\theta_i = 33.59^\circ$; (**e**) $\theta_i = 33.63^\circ$; (**f**) $\theta_i = 33.73^\circ$.

Figure 7 shows the spatial intensity profiles depending on the transverse x coordinate for different incidence angles at a distance of z = 11 cm from the grating surface.

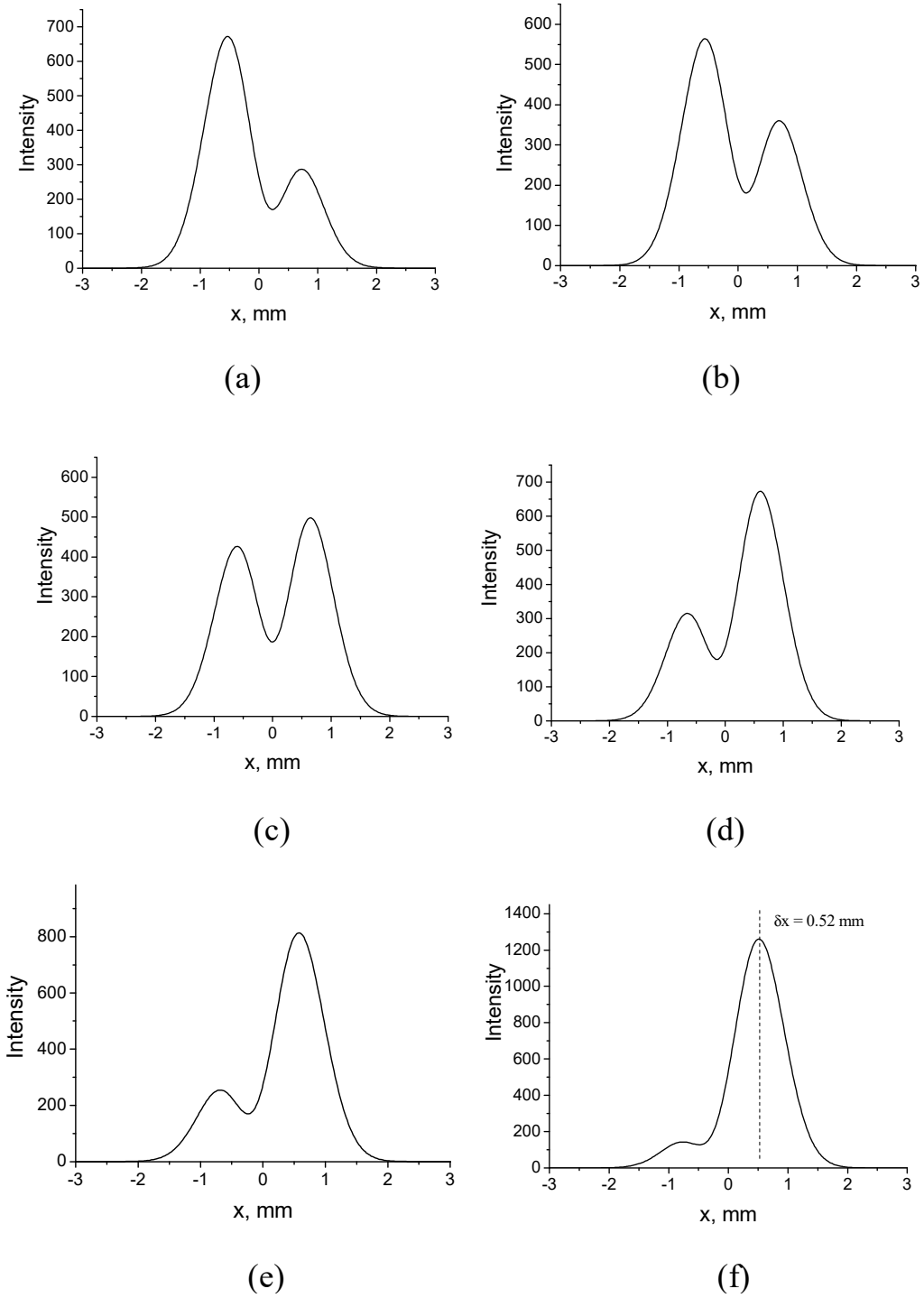

Figure 7. Calculated spatial intensity profiles of the reflected beams. z = 11 cm; incident beam FWHM = 26.64 μm. (**a**) $\theta_i = 33.43^\circ$; (**b**) $\theta_i = 33.47^\circ$; (**c**) $\theta_i = 33.53^\circ$; (**d**) $\theta_i = 33.59^\circ$; (**e**) $\theta_i = 33.63^\circ$; (**f**) $\theta_i = 33.73^\circ$.

The appearance of two peaks around the incidence resonant angle is due to the presence of a dip in the reflectivity curve (Figure 2). While the central part of the dip with a minimum reflection coefficient leads to the disappearance of the reflected light of the incident Gaussian beam, the left and right sides of the dip with a higher reflectivity lead to

the creation of two peaks. Two equal peaks appear when the angle of incidence is equal to the resonance angle.

Angular GH shift and reshaping of the reflected beam is due to intensity and phase redistribution caused by the SPR. For a Gaussian beam with a certain width in k_x, the absorption on the plasmon depends on the wavevector k_x or angle θ. Since the distribution over k_x is multiplied by reflection coefficient with a minimum at the center of the resonance (Figure 2), the result is a distribution with two peaks.

The angular spectrum components of a Gaussian beam incident at a plasmon resonance angle θ_p is located in the region

$$\theta_p - \lambda/\pi w_0 < \theta < \theta_p + \lambda/\pi w_0. \tag{2}$$

This means that the incident beam wave vectors at a resonance condition are located in the region

$$k_p - 2/w_0 < k_x < k_p + 2/w_0, \tag{3}$$

where $k_p = k_0 sin\theta_p$.

Note that the angular distance between two peaks is determined by the value $\lambda/\pi w_0$, i.e., the narrower the beam, the greater the distance between the peaks.

At a resonant angle of incidence of a wide beam (an angular spectrum range is narrower than the dip width), the splitting of the reflected beam is not observed (Figure 8a). However, there is a spatial negative displacement of the beam (Figure 8b). It follows from the wave-vector matching condition (1) that the plasmon mode is excited in -1 diffraction order of the incident beam. This indicates that, under resonance conditions, the plasmon wave moves on the grating in a negative direction [10]. Accordingly, the part of the incident beam energy is shifted backwards. The plasmon wave, in turn, is in resonance with the wave reflected in the zero order and begins to radiate into this wave (to pump energy into the reflected wave), but since the radiation does not occur instantly and the plasmon wave has a noticeable path length, the maximum of the re-emitted wave is shifted along the longitudinal coordinate x in the direction of the plasmon wave propagation.

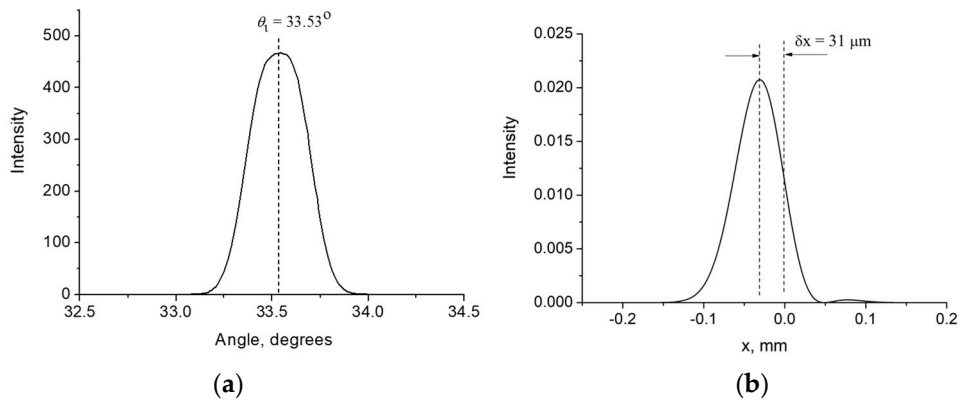

Figure 8. Reflected intensity profiles as function of the reflection angle (**a**) and transverse coordinate (**b**). Incident beam with FWHM = 66.7 μm; $\theta_i = 33.53^\circ$; z = 0.

In Figure 9, the calculated angular GH shifts depending on the angle of incidence for different beam widths are presented. The negative shifts can be observed for the incidence angles that are smaller than the critical one and the positive shifts for the angles that are greater than the critical one. It can be seen that a significant increase in the GH shift occurs near the critical angle corresponding to the Wood anomaly. The visible negative shifts can be observed near the Rayleigh anomaly for the focused beams. It follows that the higher angular shifts occur for the beams with a smaller width near the surface plasmon resonance.

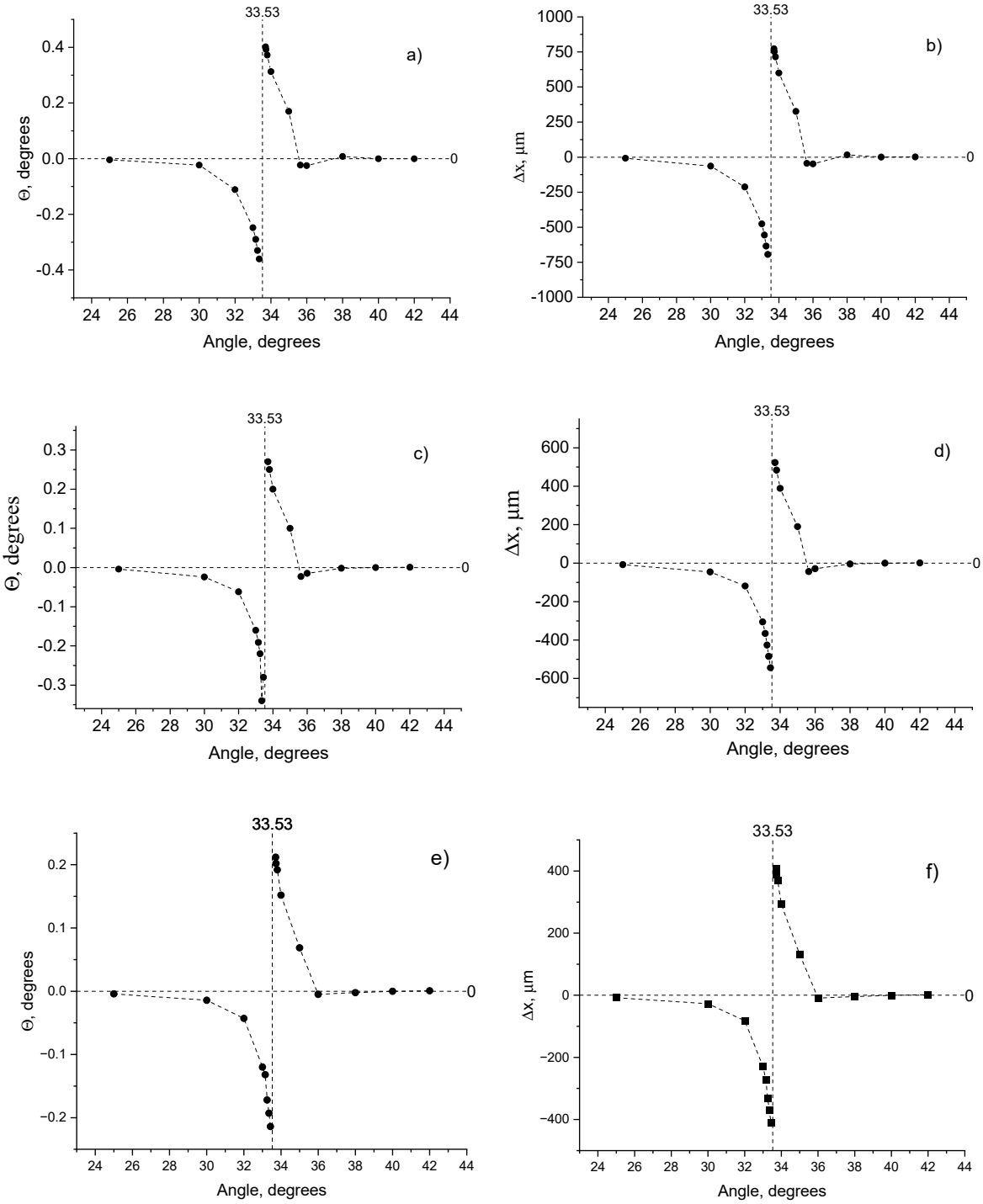

Figure 9. Calculated GH shifts (dots) as function of the incident angle: (**a**,**c**,**e**)—angular shifts; (**b**,**d**,**f**)—lateral GH shifts at z = 11 cm. h = 80 nm; FWHM = 20 μm (**a**,**b**); FWHM = 26.64 μm (**c**,**d**); FWHM = 32 μm (**e**,**f**). The calculated dots are connected by the dashed line.

Figure 10 shows the GH shifts depending on the angle of incidence for the grating depth that differs from the optimal one. It follows that the values of the angular GH shifts decrease significantly if the grating depth is not optimal for the effective coupling of the incident wave to the SP wave. In contrast to the case of the optimal depth h = 80 nm (Figure 9c,d), the GH shifts decrease by about 10 times. This indicates a significant role of SP resonance in the enhancement of the GH shift.

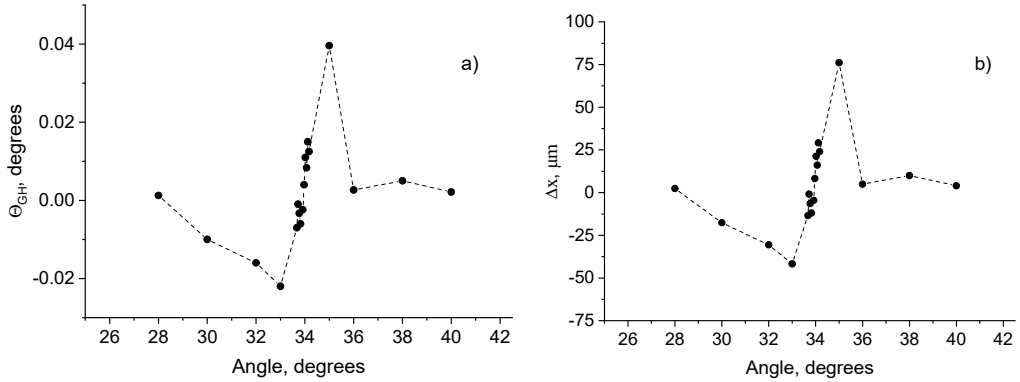

Figure 10. Calculated GH shifts (dots) as function of the incident angle: (**a**)—angular shift; (**b**)—GH shift at z = 11 cm. h = 40 nm; FWHM = 26.64 μm.

3. Measurement of the Angular GH Shift

In Figure 11 the experimental setup consisting of the He-Ne laser, half-wave plate, focusing lens, subwavelength grating and Thorlabs CCD camera beam profiler is presented. The measurements show that no GH shift for an s-polarized beam, and the effect of the reflected beam shape changing.

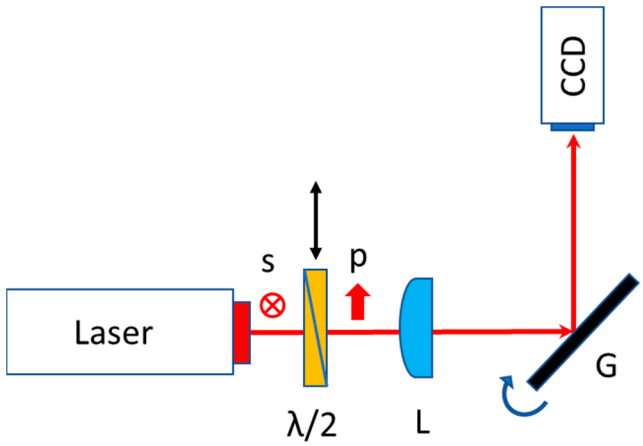

Figure 11. Experimental setup. λ/2—half-wave plate, L—lens, G—grating.

The adjustment of all these devices and optical elements and the choice of the distances between them were carried out in accordance with the simulation results. The change in the reflected beam radius with distance z is determined by the expression:

$$w(z) = w_0\sqrt{1+\left(\frac{\lambda z}{\pi w_0^2}\right)^2}, \tag{4}$$

where w_0 is the radius of the laser beam where the intensity is $1/e^2$.

The radius of the beam $w(z)$ is related to the full width at half maximum (FWHM) of the intensity distribution according to: $\mathrm{FWHM}(z) = \sqrt{2ln2}\cdot w(z)$. For the He-Ne laser beam with an initial waist of D = 0.75 mm, a wavelength λ = 632.8 nm and a focusing lens with a focal length of f = 50 mm, we have a focusing spot with a radius of 27 μm:

$$w_0 = 0.64\frac{\lambda}{D}f = 0.64\frac{0.63}{750}50\cdot 10^3 \sim 27\ \mu\mathrm{m}$$

This value corresponds to the FWHM = 32 μm. In Figure 12, the incident beam intensity profile at a lens focal plane is presented.

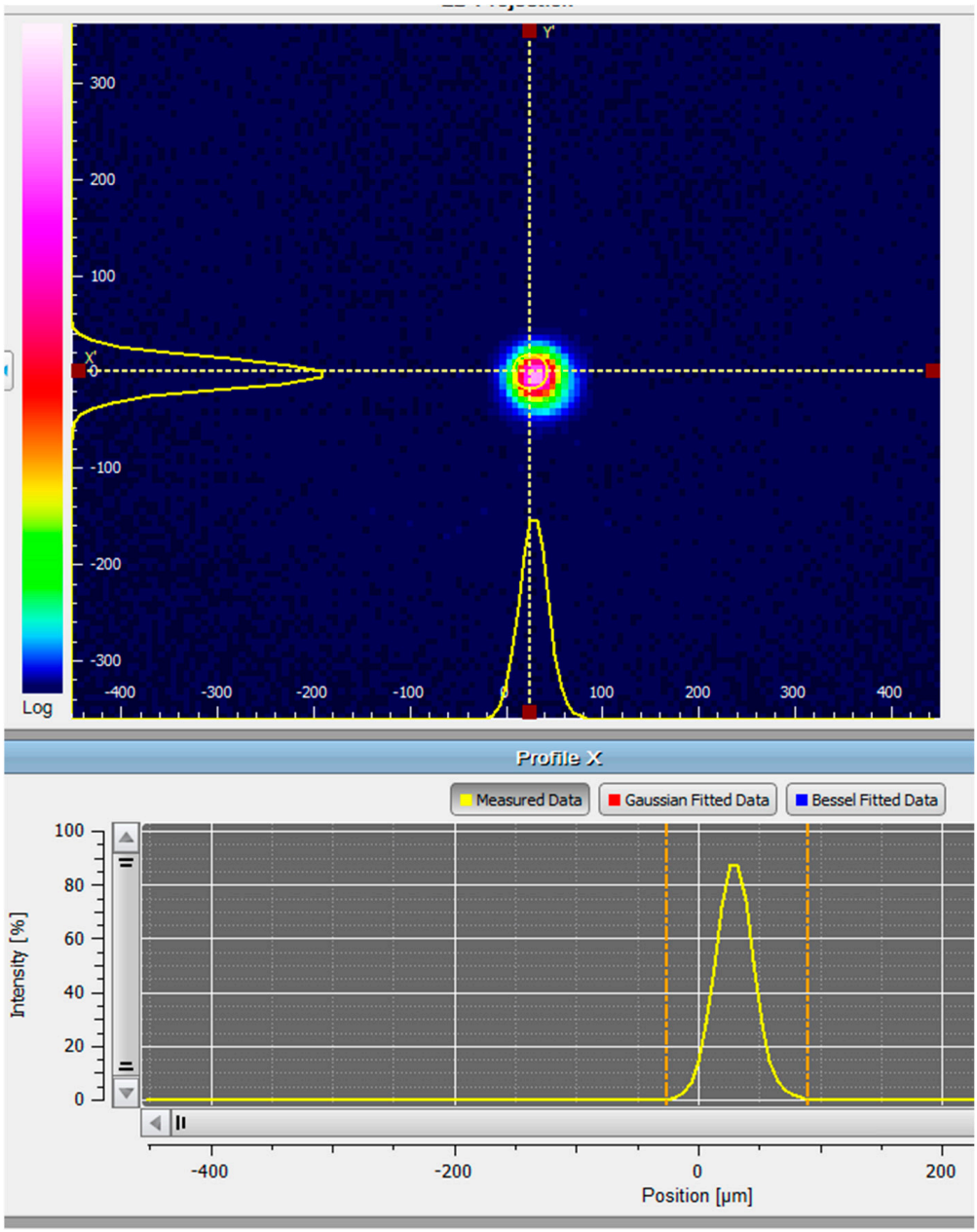

Figure 12. Incident bean intensity profile at a focal plane. f = 50 mm, z = 50 mm, FWHM = 32 µm.

Note, that the measurements include both spatial and angular shifts. While the contribution of the angular GH shift increases linearly as the beam propagates in accordance with $\Delta x = z \cdot \tan(\delta\theta) \approx z \cdot \delta\theta$, the lateral GH shift D is constant with the propagation distance z (Figure 13).

Our measurements were carried out at the distances where the spatial shift is much smaller than the angular displacement, i.e., $D \ll \Delta x$. Indeed, when spatial shifts are only of the order of a few tens of micrometers, the displacements caused by angular shift are of the order of a millimeter at a distance of 10 cm.

It is of interest to evaluate the effect of defocusing on the GH shift when a slight discrepancy between the focusing plane and the grating surface appears because of an inaccurate choice of the distance between the source and the grating surface. It follows from the simulation and measurements that the mismatch of the focusing plane with the grating surface of less than 1 mm does not have a noticeable effect on the GH shift. It is known that there is no significant change in the width and curvature of the wavefront within the depth

of focus. Indeed, the focusing depth of a Gaussian beam is determined by the Rayleigh distance or Rayleigh range, which, in our case, is equal to $Z_R = \pi w_0^2/\lambda \approx 3.6$ mm.

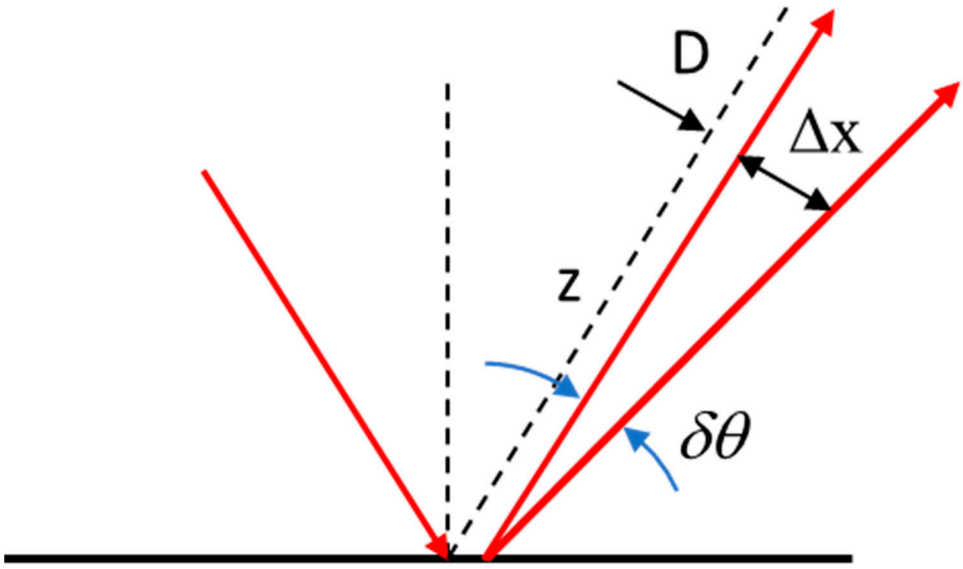

Figure 13. Reflection of an incident beam at a diffraction grating.

The GH shifts are determined by comparing the positions of the peaks of the reflected beams with *s*- and *p*-polarizations. Note that the reflection angle of the *s*-polarized beam is equal to the incidence angle, while the *p*-polarized beam deviates from the Fresnel angle of reflection.

In Figure 14, the measured intensity profiles for different angles of incidence are presented at the distance z = 11 cm from the grating surface.

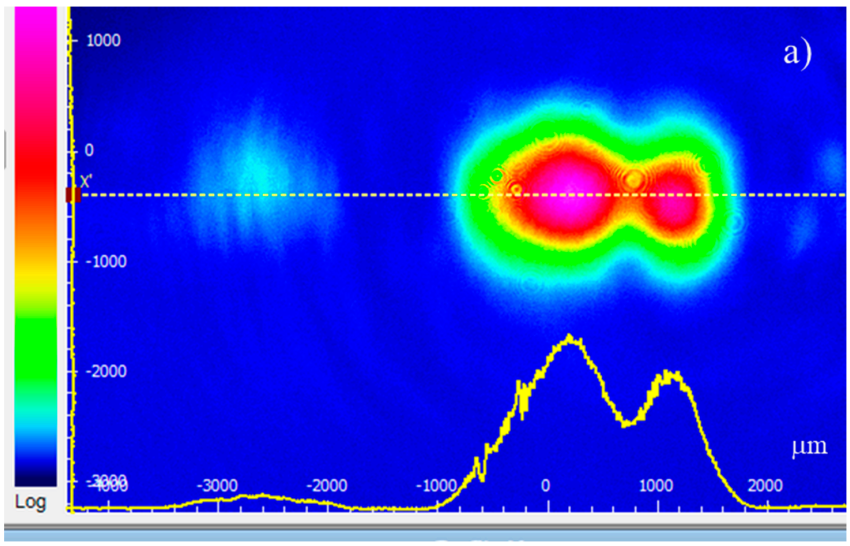

Figure 14. *Cont.*

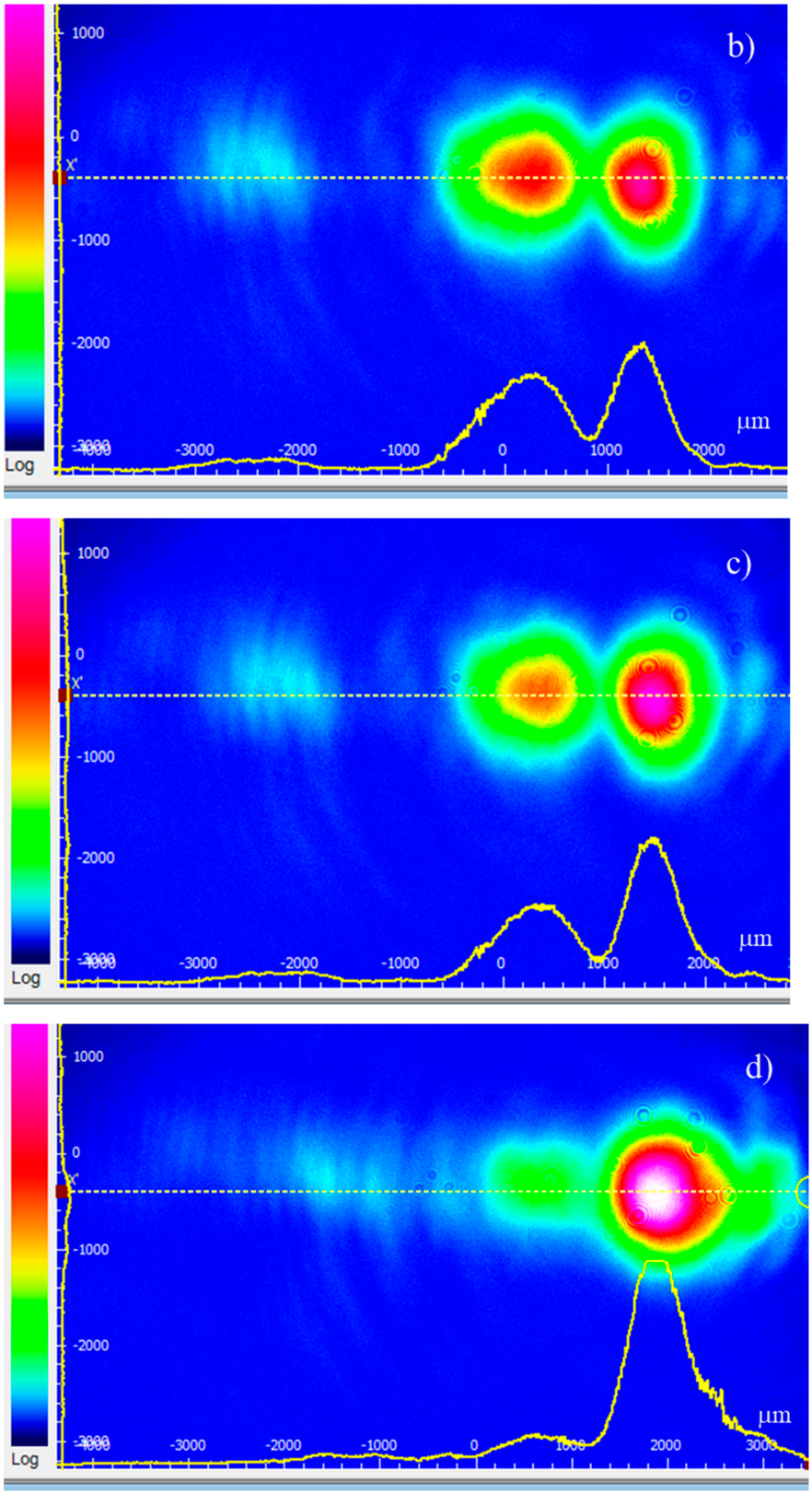

Figure 14. Measured intensity profiles of the reflected beams from the *Ni* grating with a period of $\Lambda = 400$ nm and depth of $h = 80$ nm at a distance $z = 11$ cm. (**a**) $\theta_i = 33.47^\circ$; (**b**) $\theta_i = 33.53^\circ$; (**c**) $\theta_i = 33.58^\circ$; (**d**) $\theta_i = 33.73^\circ$.

It follows from the measurements that splitting into two beams separated by an angular shift occurs for the focused beam incident at a SPR angle (Figure 14c). The high sensitivity of the GH angular shift to the light beam incidence angle near the surface plasmon resonance is demonstrated. It is seen that the reshaping of the beam profile from the Gaussian one or splitting it into two beams takes place when the incident angle is close to the plasmon resonance condition. The beam width and grating depth are the parameters that significantly affect the reflected beam profile. With the precise resonance, two equal peaks in the angular intensity distribution are observed (Figure 14b). This indicates that the subwavelength grating can work as a beam splitter. The transition between the positive and negative shifts is observed by the variation of the angle of incidence. The deviation of the incidence angle in one direction or another from the resonant angle leads to the appearance of asymmetry in the intensity distribution. There are visible changes in the reflected beam shape when the incidence angle changes even by 1 angular minute.

In Figure 15 the calculated spatial intensity profiles depending on the transverse x coordinate for different incidence angles at the distance z = 11 cm from the grating surface are presented.

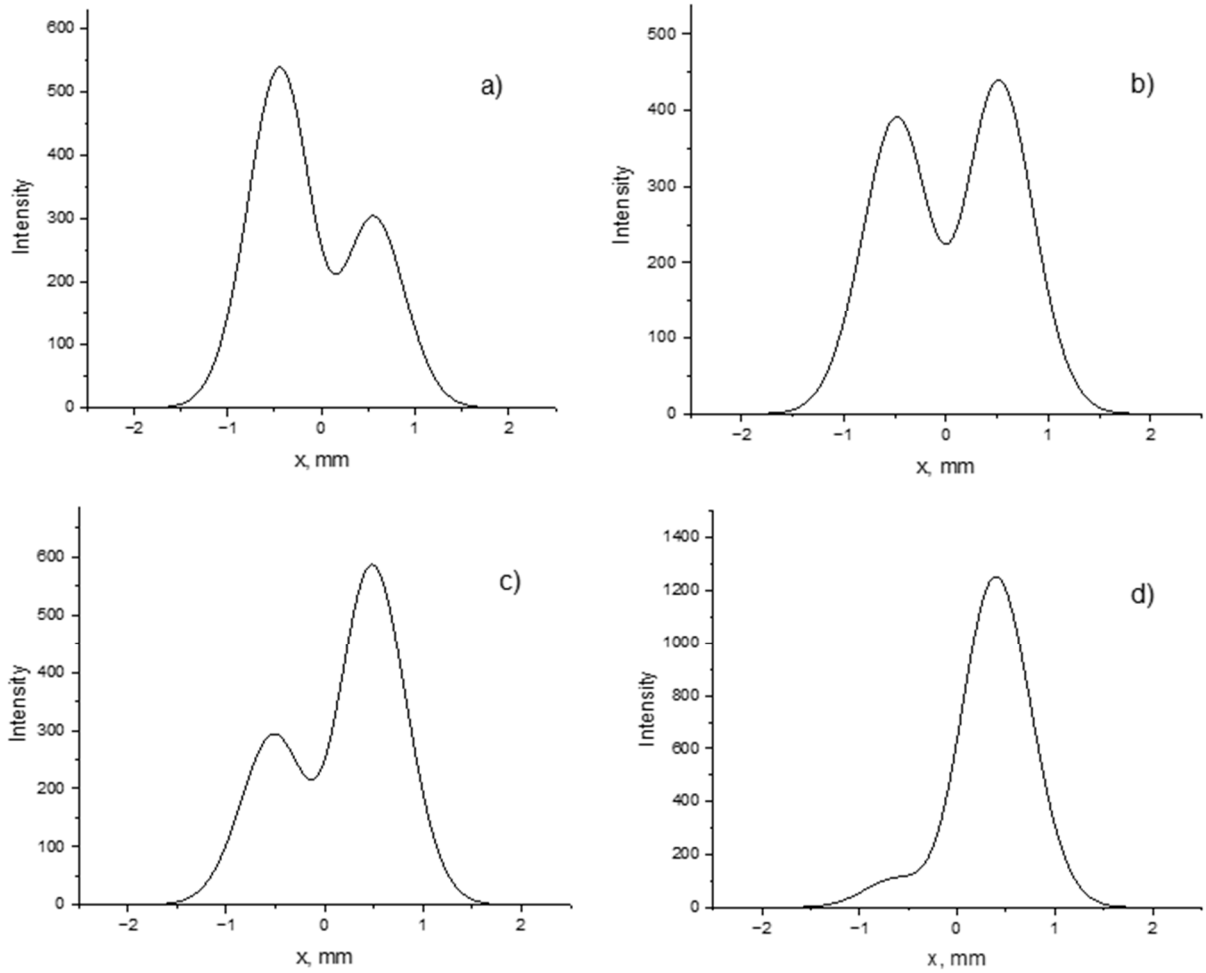

Figure 15. Calculated intensity profiles of the reflected beams from the *Ni* grating with a period of Λ = 400 nm and depth of h = 80 nm at a distance z = 11 cm. (**a**) $\theta_i = 33.47^\circ$; (**b**) $\theta_i = 33.53^\circ$; (**c**) $\theta_i = 33.58^\circ$; (**d**) $\theta_i = 33.73^\circ$.

It follows from the numerical calculations that the beam profiles and GH shifts for various incidence angles are in good agreement with the experiment. It can also be seen that the calculated widths of the reflected beams are equal to the measured values. A significant change in the beam shape occurs when the beam is incident under resonance

condition. However, the Gaussian shape persists after the reflection of the incident beam from the grating surface outside the region $\theta_p - \lambda/\pi w_0 < \theta < \theta_p + \lambda/\pi w_0$. In Figure 16, the measured intensity profiles for various angles of incidence that are located outside the region $\theta_p - \lambda/\pi w_0 < \theta < \theta_p + \lambda/\pi w_0$, at the distance z = 11 cm from the grating surface are presented.

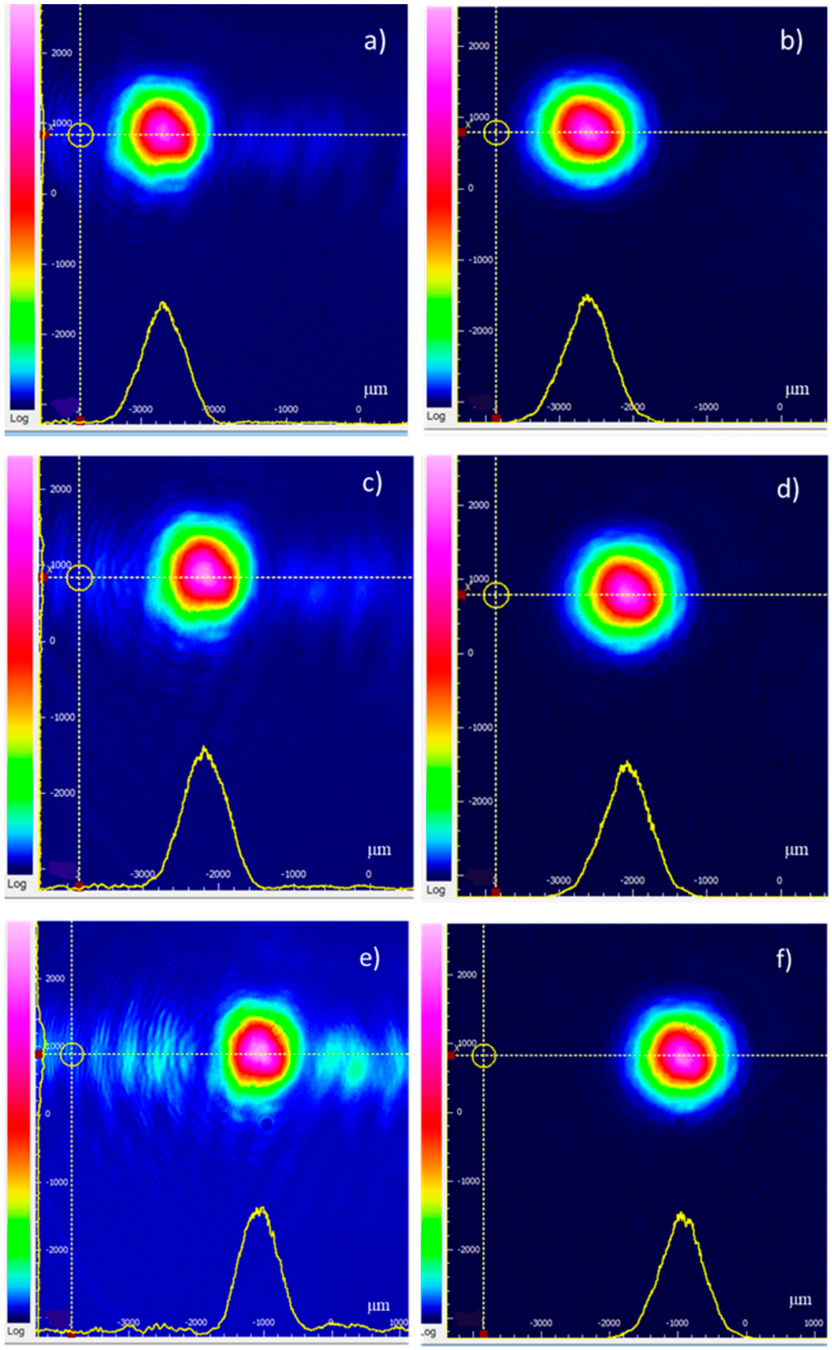

Figure 16. Measured intensity profiles of the reflected beams from the *Ni* grating with the period Λ = 400 nm and the depth h = 80 nm at the distance z = 11 cm. (**a**,**b**) $\theta_i = 32.00^\circ$, Δx = −78 µm; (**c**,**d**) $\theta_i = 32.17^\circ$, Δx = −115 µm; (**e**,**f**) $\theta_i = 32.50^\circ$, Δx = −181 µm. Left column—*p*-polarization; right column—*s*-polarization.

In Table 1 the theoretical and experimental results are presented for different incident angles.

Table 1. Angular GH shifts at different incidence angles. h = 80 nm, FWHM = 32 μm.

Incidence angle, deg	32.00	33.00	33.43	33.71	33.73	34.00	35.00
Θ_{GH}, deg μrad theory	−0.043 −753	−0.12 −2100	−0.214 −3745	0.212 3710	0.202 3535	0.152 2664	0.0686 1200
Θ_{GH}, deg μrad experiment	−0.0405 −709	−0.11 −1910	−0.198 −3464	0.224 3927	0.201 3509	0.161 2809	0.064 1118
GH, μm; z = 11 cm theory	−82	−230	−410	408	389	293	132
GH, μm; z = 11 cm experiment	−78	−210	−381	432	386	309	123

In the experiment, an angular shift of 0.30 degrees (0.5×10^{-2} rad) was demonstrated for a nickel grating under SPR, which is confirmed by modeling. Note that the increase in the angular shift is almost 100 times compared to the known results obtained for the diffraction grating [22]. Such an increase in the angular deviation is achieved by the appropriate adjustment of the grating depth to achieve the optimal SP coupling condition. A visible transformation of the reflected beam shape is observed when the angle of incidence changes by a small amount. Even 1 angular minute (3×10^{-4} rad) change in the incidence angle causes a noticeable reshaping of the reflected beam profile.

It follows that the measured angular GH shifts are in excellent agreement with the simulation results.

4. Discussion

Thus, the effect of angular GH shift for a visible light beam under the excitation of surface plasmon resonance (SPR) in a metal subwavelength grating is investigated using rigorous electromagnetic calculations and direct measurements. The SPR enhanced negative and positive angular GH shifts are demonstrated for the reflected beam from the grating with optimal depth. The high sensitivity of the GH shift and beam reshaping to the angle of incidence of the focused light beam near SPR is experimentally demonstrated.

It can be seen that the simulation results are in good agreement with the measurements. The numerical simulation with a Gaussian beam demonstrates the effects of the GH shift and beam reshaping observed in the experiment. The presence of negligible differences between the simulated and experimentally measured GH shifts can be due to the deviations of the grating profile from the sinusoidal one and due to surface roughness on the metal grating. In [29], the effect of the surface roughness on the of a metal grating for SPR sensors was demonstrated. It was shown in [30] that the SPR sensors based on a trapezoidal grating have great resistance to changes in grating parameters and relatively high performance.

Currently, there are various results of measurements of angular GH shifts of a Gaussian optical beam reflected at the air–glass interface near the Brewster angle [14], at the glass–air interface [19], at the air–Au interface [18], at the prism–Au interface in the Kretschmann configuration [31] and in a grating structure [22]. Angular shifts of 60 μrad were observed in [18] for a beam waist of 169 μm at a critical angle of incidence. In [14], it was found that the measured angular deviation ranges from 10 to 10^4 μrad. Angular GH shifts up to 5×10^3 μrad were observed at the prism-Au interface when the incident beam was tightly focused to a 5 μm beam waist [31]. Angular GH shifts of the order of several hundred micrometers were demonstrated for a focused beam using a simple gold (Au) film on a substrate to excite surface plasmons [22]. Here we present the first results of observing the angular GH shifts of the light beam incident on a metal subwavelength grating.

Although the physical aspects of the GH shifts are well described in many publications, the effect of the beam width and grating depth on the GH shift near the surface plasmon resonance in subwavelength gratings has not yet been studied.

We found that the values of the spatial shift and angular deviation in the incidence plane depend on the parameters of the subwavelength grating (period and depth), as well

as on the incident beam width. It is evident that both the spatial displacement of the beam and its angular deviation from the Fresnel reflection angle are present in the measurements. However, the displacement of the beam center on the profilometer screen mainly due to the effect of angular deviation.

Future research can be related to the consideration of the GH shifts of vortex beams [32] and the influence of the spatial coherence on the GH shift [33]. Of particular interest is the consideration of structured vortex beams with an orbital angular momentum [34–36] and the effect of polarization on the GH shift [37,38].

5. Conclusions

In summary, the angular GH shift near SPR in subwavelength grating is investigated using rigorous electromagnetic calculations and direct measurements. The extremely large negative and positive angular GH shifts enhanced by surface plasmon resonance are demonstrated for the reflected beam from the grating with optimal depth. It is shown that the reflected beam splits into two angularly separated beams with large negative and positive angular shifts. The angular distance between the intensity peaks increases with decreasing width of the incident beam. There is no beam splitting effect for the angles of incidence beyond the surface plasmon region. The high sensitivity of the Goos-Hanchen shift and beam reshaping to the light beam incidence angle near the surface plasmon resonance is demonstrated. This indicates that a tunable GH shift and a change in the reflected beam shape can be observed by the variation of the angle of incidence near the surface plasmon resonance in subwavelength gratings with optimal depth.

The results can be useful in the development of various sensors [31,39–42] and optical switches, as well as in angular metrology and in enhancing the sensitivity of measurements in gravitational wave detection [43].

Author Contributions: Conceptualization, N.I.P.; methodology, N.I.P.; software and simulation, B.A.U.; grating design and fabrication, V.A.D. and V.V.P.; experimental analysis, Y.M.S. and V.V.S.; writing—original draft preparation, N.I.P.; writing—review and editing, N.I.P. and B.A.U.; supervision, N.I.P.; project administration, N.I.P.; funding acquisition, N.I.P. All authors have read and agreed to the published version of the manuscript.

Funding: This research was funded by Russian Foundation for Basic Research, grant number 19-29-11026 and Ministry of Science and Higher Education of the Russian Federation, grant number FFNS-2022-0009.

Institutional Review Board Statement: Not applicable.

Informed Consent Statement: Not applicable.

Data Availability Statement: Not applicable.

Conflicts of Interest: The authors declare no conflict of interest.

References

1. Goos, F.; Hanchen, H. Ein neuer und fundamentaler Versuch zur Total reflexion. *Ann. Der Phys.* **1947**, *436*, 333–346. [CrossRef]
2. Tamir, T.; Bertoni, H.L. Lateral displacement of optical beams at multilayered and periodic structures. *J. Opt. Soc. Am.* **1971**, *61*, 1397–1413. [CrossRef]
3. Merano, M.; Aiello, A.; Hooft, G.W.; van Exter, M.P.; Eliel, E.R.; Woerdman, J.P. Observation of Goos-Hanchen shifts in metallic reflection. *Opt. Express* **2007**, *15*, 15928–15934. [CrossRef] [PubMed]
4. Schreier, F.; Schmitz, M.; Bryngdahl, O. Beam displacement at diffractive structures under resonance conditions. *Opt. Lett.* **1998**, *23*, 576–578. [CrossRef] [PubMed]
5. Bonnet, C.; Chauvat, D.; Emile, O.; Bretenaker, F.; Floch, A.L.; Dutriaux, L. Measurement of positive and negative Goos–Hänchen effects for metallic gratings near Wood anomalies. *Opt. Lett.* **2001**, *26*, 666–668. [CrossRef] [PubMed]
6. Yin, X.; Hesselink, L.; Liu, Z.; Fang, N.; Zhang, X. Large positive and negative lateral optical beam displacements due to surface plasmon resonance. *Appl. Phys. Lett.* **2004**, *85*, 372–374. [CrossRef]
7. Soboleva, I.V.; Moskalenko, V.V.; Fedyanin, A.A. Giant Goos-Hanchen effect and Fano resonance at photonic crystal surfaces. *Phys. Rev. Lett.* **2012**, *108*, 123901. [CrossRef]

8. Wang, L.; Chen, H.; Zhu, S. Large negative Goos-Hänchen shift from a weakly absorbing dielectric slab. *Opt. Lett.* **2005**, *30*, 2936–2938. [CrossRef]
9. Kong, Q.; Shi, H.; Shi, J.; Chen, X. Goos-Hänchen and Imbert-Fedorov shifts at gradient metasurfaces. *Opt. Express* **2019**, *27*, 11902. [CrossRef]
10. Petrov, N.I.; Danilov, V.A.; Popov, V.V.; Usievich, B.A. Large positive and negative Goos-Hänchen shifts near the surface plasmon resonance in subwavelength grating. *Opt. Express* **2020**, *28*, 7552–7564. [CrossRef]
11. Beenakker, C.W.J.; Sepkhanov, R.A.; Akhmerov, A.R.; Tworzydlo, J. Quantum Goos-Hänchen Effect in Graphene. *Phys. Rev. Lett.* **2009**, *102*, 146804. [CrossRef] [PubMed]
12. Wan, R.; Zubairy, M.S. Tunable and enhanced Goos-Hänchen shift via surface plasmon resonance assisted by a coherent medium. *Opt. Express* **2020**, *28*, 6036. [CrossRef] [PubMed]
13. Petrov, N.I. Beam shift in a graded-index optical fiber. *J. Opt.* **2013**, *15*, 014011. [CrossRef]
14. Merano, M.; Aiello, A.; van Exter, M.P.; Woerdman, J.P. Observing angular deviations in the specular reflection of a light beam. *Nat. Photonics* **2009**, *3*, 337–340. [CrossRef]
15. Petrov, N.I. Reflection and transmission of strongly focused light beams at a dielectric interface. *J. Mod. Opt.* **2005**, *52*, 1545–1556. [CrossRef]
16. Wong, Y.P.; Miao, Y.; Skarda, J.; Solgaard, O. Large negative and positive optical Goos–Hänchen shift in photonic crystals. *Opt. Lett.* **2018**, *43*, 2803–2806. [CrossRef]
17. Jiang, Q.; Chen, J.; Liang, B.; Wang, Y.; Hu, J.; Zhuang, S. Direct measurement of the negative Goos–Hänchen shift of single reflection in a two-dimensional photonic crystal with negative refractive index. *Opt. Lett.* **2017**, *42*, 1213–1216. [CrossRef]
18. Aiello, A.; Merano, M.; Woerdman, J.P. Duality between spatial and angular shift in optical reflection. *Phys. Rev. A* **2009**, *80*, 061801(R). [CrossRef]
19. Santana, O.J.S.; de Araujo, L.E.E. Direct measurement of the composite Goos–Hänchen shift of an optical beam. *Opt. Lett.* **2018**, *43*, 4037–4040. [CrossRef]
20. De Leo, S.; Maggio, L.; d'Ambrosio, M. Goos–Hänchen Lateral Displacements and Angular Deviations: When These Optical Effects Offset Each Other. *Photonics* **2022**, *9*, 643. [CrossRef]
21. Xu, Y.; Wu, L.; Ang, L.K. Ultrasensitive Optical Temperature Transducers Based on Surface Plasmon Resonance Enhanced Composited Goos-Hänchen and Imbert-Fedorov Shifts. *IEEE J. Sel. Top. Quantum Electron.* **2021**, *27*, 4601508. [CrossRef]
22. Yallapragada, V.J.; Ravishankar, A.P.; Mulay, G.L.; Agarwal, G.S.; Achanta, V.G. Observation of giant Goos-Hänchen and angular shifts at designed metasurfaces. *Sci. Rep.* **2016**, *6*, 19319. [CrossRef]
23. Lyndin, N.M.; Usievich, B.A. MC Grating Program. Available online: https://mcgrating.com (accessed on 26 January 2023).
24. Petrov, N.I.; Nikitin, V.G.; Danilov, V.A.; Popov, V.V.; Usievich, B.A. Subwavelength diffractive color beam combiner. *Appl. Opt.* **2014**, *53*, 5740–5744. [CrossRef]
25. Petrov, N.I.; Danilov, V.A.; Popov, V.V.; Usievich, B.A. Visible-range subwavelength diffraction gratings. *Quant. Electron.* **2018**, *48*, 537–544. [CrossRef]
26. Maradudin, A.A.; Simonsen, I.; Polanco, J.; Fitzgerald, R.M. Rayleigh and Wood anomalies in the diffraction of light from a perfectly conducting reflection grating. *J. Opt.* **2016**, *18*, 024004. [CrossRef]
27. Raether, H. *Surface Plasmons on Smooth and Rough Surfaces and on Gratings*; Springer: Berlin, Germany, 1988.
28. Cheng, Y.C.; Zeng, H.; Trull, J.; Cojocaru, C.; Malinauskas, M.; Jukna, T.; Wiersma, D.S.; Staliunas, K. Beam focalization in reflection from flat dielectric subwavelength gratings. *Opt. Lett.* **2014**, *39*, 6086–6089. [CrossRef]
29. Bruhier, H.; Verrier, I.; Gueye, T.; Varenne, C.; Ndiaye, A.; Parriaux, O.; Veillas, C.; Reynaud, S.; Brunet, J.; Jourlin, Y. Surface plasmons propagation along metallic rough diffraction gratings. *Proc. SPIE* **2022**, *12131*, 9–16.
30. Chai, Y.; Li, F.; Wang, J.; Karvinen, P.; Kuittinen, M.; Kang, G. Enhanced sensing performance from trapezoidal metallic gratings fabricated by laser interference lithography. *Opt. Lett.* **2022**, *47*, 1009–1012. [CrossRef] [PubMed]
31. Olaya, C.M.; Hayazawa, N.; Hermosa, N.; Tanaka, T. Angular Goos−Hänchen shift sensor using a gold film enhanced by surface plasmon sonance. *J. Phys. Chem. A* **2021**, *125*, 451–458. [CrossRef]
32. Kan, X.F.; Zou, Z.X.; Yin, C.; Xu, H.P.; Wang, X.P.; Han, Q.B.; Cao, Z.Q. Continuous Goos-Hänchen Shift of Vortex Beam via Symmetric Metal-Cladding Waveguide. *Materials* **2022**, *15*, 4267. [CrossRef]
33. Zhu, G.; Gao, B.; Zhang, J.; Wang, L.G. Experimental proof on the effect of beam width and spatial coherence on Goos-Hanchen shift. *Opt. Laser Technol.* **2023**, *159*, 109027. [CrossRef]
34. Petrov, N.I. Vector and Tensor Polarizations of Light Beams. *Las. Phys.* **2008**, *18*, 522–525. [CrossRef]
35. Petrov, N.I. Spin-orbit and tensor interactions of light in inhomogeneous isotropic media. *Phys. Rev. A* **2013**, *88*, 023815. [CrossRef]
36. Petrov, N.I. Vector Laguerre–Gauss beams with polarization-orbital angular momentum entanglement in a graded-index medium. *J. Opt. Soc. Am. A* **2016**, *33*, 1363–1369. [CrossRef]
37. Petrov, N.I. Depolarization of Light in Optical Fibers: Effects of Diffraction and Spin-Orbit Interaction. *Fibers* **2021**, *9*, 34. [CrossRef]
38. Petrov, N.I. Depolarization of vector light beams on propagation in free space. *Photonics* **2022**, *9*, 162. [CrossRef]
39. Wang, X.; Yin, C.; Sun, J.; Li, H.; Wang, Y.; Ran, M.; Cao, Z. High-sensitivity temperature sensor using the ultrahigh order mode-enhanced Goos-Hänchen effect. *Opt. Express* **2013**, *21*, 13380. [CrossRef]
40. Han, X.; Liu, K.; Sun, C. Plasmonics for Biosensing. *Materials* **2019**, *12*, 1411. [CrossRef]

41. Chen, J.; Zeng, Y.; Zhou, J.; Wang, X.; Jia, B.; Miyan, R.; Gu, Y. Optothermophoretic flipping method for biomolecule interaction enhancement. *Biosens. Bioelectron.* **2022**, *204*, 114084. [CrossRef]
42. Miyan, R.; Wang, X.; Zhou, J.; Zeng, Y.; Qu, J.; Ho, H.P.; Shao, Y. Phase interrogation surface plasmon resonance hyperspectral imaging sensor for multi-channel high-throughput detection. *Opt. Exp.* **2021**, *29*, 31418–31425. [CrossRef]
43. Petrov, N.I.; Pustovoit, V.I. Small-sized interferometer with Fabry-Perot resonators for gravitational wave detection. *Sensors* **2021**, *21*, 1877. [CrossRef] [PubMed]